Convolutive Voltammetry and Digital Simulation Examination of Ferric Chloride at a Gold Electrode

A. A. Al-Owais[1] and I. S. El-Hallag[*2]

[1]*Chemistry Department, Colleague of Science, King Saud University, Saudi Arabia*
[2] *Chemistry Department, Faculty of Science, Tanta University, Tanta, Egypt*
Corresponding author: i.elhallag@yahoo.com

Received 08/05/2023; accepted 25/11/2023
https://doi.org/10.4152/pea.2025430201

Abstract
In this study, employing an accurate and simple method of CvV and DV, combined with numerical simulation, $FeCl_3$ was electrochemically examined in a 1 M HCl aqueous solution using Au working electrode. It was discovered that electrons exchange between Fe (III) and Fe (II) was a quasi-reversible process. CV was used to determine the electrochemical parameters of Fe (III)/Fe (II), such as D, E^o, k_s and α values, which were then confirmed using a numerical simulation method. The nature of $K_3[Fe(CN)_6]$ electrode reaction, in selected media at Au electrodes, was studied. It was determined that its mechanism occurred through moderately fast electrons transfer.

Keywords: DV; CvV; CV; $FeCl_3$; numerical simulation.

Introduction•

Iron is a transition metal with the symbol Fe and atomic number 26. It is the most common element on Earth. Fe is a necessary component involved in various metabolic processes, including O transport, DNA synthesis, and energy production for electrons transport [1]. An insufficient supply of Fe to cells caused by a lack of its reserves is the most common nutritional deficiency worldwide, particularly affecting children, childbearing age and pregnant women [2]. Fe deficiency may cause the development of anemia, and result in functional impairments affecting cognitive development and immunity mechanisms, as well as infant or maternal mortality, if it occurs during pregnancy [1]. The main therapeutic preparation of Fe is $FeSO_4$, and Fe-sucrose may also be given intravenously [3]. Fe exists in two oxidation states: Fe (II) and Fe (III). NHFe in food is mainly in Fe (III) state, which is its insoluble form and must be reduced to Fe (II) for absorption [3]. When Fe (III) is converted to soluble Fe (II), it primarily exists in the circulation in complex forms bound to proteins (hemoprotein) as heme compounds (hemoglobin or myoglobin), heme enzymes, or NH compounds (flavin-Fe enzymes, transferring and ferritin) [1].

• The abbreviations and symbols definition lists are on pages 95-96.

Once converted, Fe (II) serves to support various biological functions. Fe promotes the synthesis of O transport proteins, such as myoglobin and hemoglobin, and the formation of heme enzymes and other Fe-containing enzymes involved in electron transfer and redox reactions [1]. It also acts as a cofactor in many NH enzymes, including hydroxylases and ribonucleotide reductase [2]. Fe-containing proteins are responsible for mediating antioxidant actions, energy metabolism, O sensing actions and DNA replication and repair [2]. Saturation of transferrin from high concentrations of unstable Fe preparations may elevate the levels of weakly transferrin-bound Fe (III), which can induce oxidative stress by catalyzing lipid peroxidation and reactive O species formation [4, 5]. Fe is incorporated into various proteins to serve biological functions as a structural component or cofactor. Once Fe (III) or Fe (II) cations from intestinal enterocytes or reticuloendothelial macrophages are bound to circulating transferrin, Fe-transferrin complex binds to the cell-surface transferrin receptor (TfR) 1, resulting in endocytosis and uptake of metal cargo. Internalized Fe is transported to the mitochondria for the synthesis of heme or Fe-S clusters, which are integral parts of several metalloproteins. Excess Fe is stored and detoxified in cytosolic ferritin [1]. Internalized Fe (II) is exported across the basolateral membrane into the bloodstream via Fe (II) ferroportin transporter, which is coupled by reoxidation to Fe (III) through membrane-bound ferroxidase hephaestin or ceruloplasmin activity [1]. Fe (III) is again scavenged by transferrin, which maintains Fe (III) in a redox-inert state and delivers it into tissues [1]. Fe (III) participates in the autoxidation reaction, where it can be chelated by DNA. It mainly binds to the backbone phosphate group, whereas at higher metal ions contents, the cation also binds to guanine N-7 atom [6]. Fe absorption and systemic Fe homeostasis are regulated by hepcidin, which is a peptide hormone that also regulates ferroportin-1 activity, which is the sole Fe-efflux protein [7]. Fe is mostly absorbed in the duodenum and upper jejunum [8, 9]. Fe (III) displays low solubility at the intestine neutral pH, and is mainly converted to Fe (II) by Fe (III) reductases [10], as Fe (III) salts are only half as well adsorbed as Fe (II) salts [11].

It has been proposed that there may be separate cellular uptake pathways for Fe (II) and Fe (III) Fe. While Fe (II) is primarily carried by divalent metal transporter-1 (DMAT-1), cellular uptake of Fe (III) is predominantly mediated by beta-3 integrin and mobilferrin, which is also referred to in some sources as a calreticulin homologue [4]. However, the most dominant pathway in humans is unclear [4].

CvV and DV are commonly applied methods to observe E^o behavior, by measuring the current generated from electrons transfer between an electrode and an electrolyte solution, as a function of changes in potential. The experiment employed a cell equipped with reference, working and auxiliary electrodes [12-17]. CvV is frequently used in applied electrochemistry, analytical electrochemistry and surface coating [12, 13, 16-18]. In contrast, there is a lack of information regarding its application in food and health fields. Previous work examined Fe (II) and Fe (III) ions redox properties upon nicotine addition, and its correlation with

neurodegenerative disease [16]. Nicotine ability to form a complex reaction with free Fe was proved by the change from reversible to quasi-reversible performances, as well as by the reduced rate of electrons transfer and apparent k_s; thus, Fe reactivity was successfully reduced [16]. Another study investigated flavonoids structure antioxidant activity towards different free radicals by FRAP, with a slight modification using 96-well microplates [17]. Their oxidation potentials were analyzed by CV, and found to be in good agreement with FRAP results [17]. Semi integral electroanalysis, which is considered a good tool for elucidating the nature of electrodes reaction, was used to investigate the electrochemical behavior of some electroactive species and determine their kinetic parameters [19-21].
The aim of the present study was to investigate the likelihood of Fe (III) reduction by CV and DV electrochemical methods combined with numerical simulation.

Experimental

Chemical compounds

From Aldrich Chemical Co., $FeCl_3$ and KNO_3 were purchased and used as bought. All chemicals were of spectral purity.

Instrumentation

CV and DV experiments were carried out utilizing the Computerized Potentiostat Model 283 and PAR Model 175 Universal System Programmer (from EG and G). Experiments were performed via an ordinary three-electrode electrochemical cell adjustment. The active Au working electrode area was $6.75 \times 10^{-3}/cm^2$. Pt wire and Ag/AgCl were used as counter and standard electrodes, respectively. Voltage was determined *vs*. Ag/AgCl electrode, at 25 ºC, with 1 mol/L HCl as supporting electrolyte. CV data were achieved at SR values ranging from 0.01 to 2 V/s^{-1}, at 25±0.5 ºC.

Numerical simulation

Computer-generation of theoretical CV is a good way to elucidate simple and complex electrode pathways, confirm and verify the nature of electrochemical reactions, and also to inspect i-E curves for many types of electrode reactions with different electrons transfer rates [22-23]. EG and G Condesim software package were used to generate theoretical CV via virtual simulation on a PC computer. The simulation process was done employing finite difference techniques.

Results and discussion

CV of a Pt electrode in 1.0 M HCl + 0.01 M $FeCl_3$, at a SR of 0.05 V/s^{-1} and 25 ºC (Fig. 1), shows a cathodic peak (E_{pc}), at 0.38 V, which is coupled with an anodic peak (E_{pa}), at 0.51 V.
The cathodic peak corresponds to Fe (III) cation reduction on the Au electrode:

$$Fe\ (III) + e^- = Fe\ (II)$$

The anodic coupled peak corresponds to formed Fe(II) cations oxidation:

$$Fe\ (II) - e^- = Fe\ (III)$$

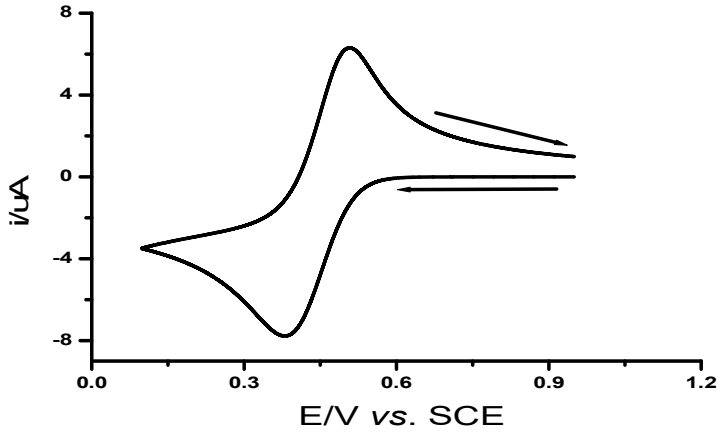

Figure 1: CV for Fe (III)/Fe (II) system (10^{-2} M) in HCl (1 M) at 25 ºC, on Au electrode.

Fig. 2 indicates CV of the investigated system at various Au electrodes.

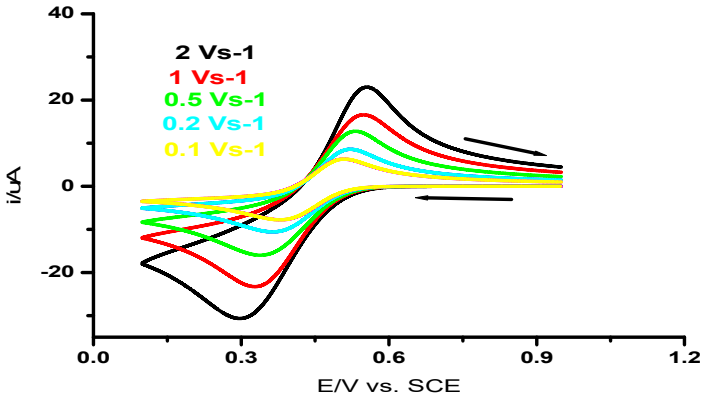

Figure 2: CV of the investigated system at various C of Au electrodes in 1 M HCl.

It is seen that I_{pc} and I_{pa} increased with increasing *v*, and i_{pa}/i_{pc} ratio of 1. As noticed, the system under study is quasi-reversible, since the criterion for fast systems was not herein satisfied ($E_{pa} - E_{pc} > 0.057$ V), but both peaks are present on the CV [24]. The half-wave potential is:

$$E_{1/2} = (E_{pc} + E_{pa})/2 \qquad (1)$$

Often interpreted as redox potential of a system, it does not depend on *v* within the measurement accuracy limits. $E_{1/2}$ determined value for Fe (III)/Fe (II) system was found to be equal 0.443 ± 0.002 V. The variation of the values of wave parameters with ν were cited in Table 1.

Table 1: CV data of 0.01 M Fe (III)/Fe (II) system at Au electrode in 1.0 M HCl with various ν for Au, at 25 ºC.

SR/υ (V/s^{-1})	E_{pa} (V)	i_{pa} (µA)	E_{pc} (V)	*ΔE_p (V)
0.05	0.39	5.7	0.500	0.108
0.1	0.377	7.70	0.505	0.128
0.2	0.357	10.18	0.519	0.162
0.5	0.357	15.60	0.532	0.188
1.0	0.234	23.12	0.549	0.225
2.0	0.291	29.38	0.553	0.259

*peak potential separation

The i_p values on i-E curves were determined by Randles–Sevcik eq.:

$$i_p = 3.0 \times 10^5 (\alpha na)^{0.5} SnC\, D^{0.5}\, v^{0.5} \qquad (2)$$

where 3.0 x 10^5 is the eq. constant at 25 ºC; n is the number of electrons involved in the redox process of Fe (III)/Fe(II) couple, which is 1; na is the number of electrons involved in the rate determining step; S is the electrode surface area (cm^2); and C is the concentration of the electrochemically active substance ($mmol/cm^{-3}$). This eq. describes redox processes that occur in equilibrium systems. However, it can also be used to describe quasi-reversible and even irreversible systems [24]. Its applicability criterion for describing the cathode process in this system is that i_{pc} *vs.* $v^{0.5}$ should be linear. Fig. 3 exhibits the linear presentation of i_{pc} *vs.* $v^{0.5}$, which confirms Fe (III)/Fe (II) system diffusion character.

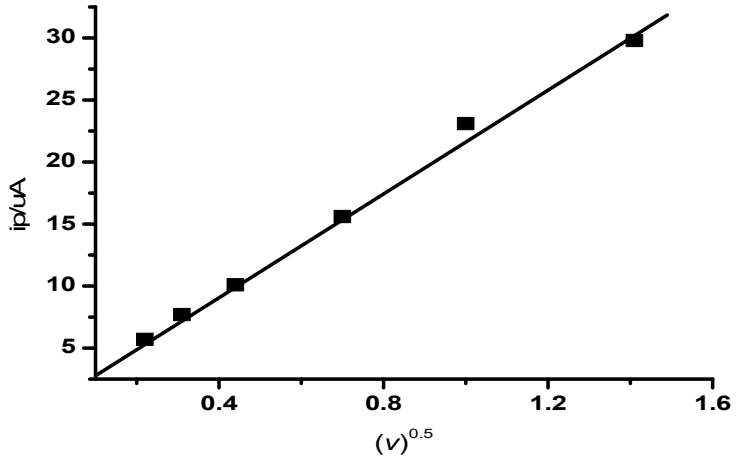

Figure 3: Plot of i_p *vs.* $v^{0.5}$ for Fe (III) /Fe (II) system in 1 M HCl, at 25 ºC, on Au electrode.

CV study indicated that Fe (III)/Fe (II) electrode reaction in aqueous media involved a quasi-reversible electrons transfer without any coupled chemical reactions. D values of Fe (III) /Fe (II) system were determined from the slope of the plot shown in Fig. 3, and found to be 4.8 x 10^{-10} m^2/s^{-1}. Peak characteristics determined from CV, at Au various C, are listed in Table 1.

CvV

The convolution transformation (I_l) of experimental i(t) data is expressed as:

$$I_l = \frac{1}{\sqrt{\pi}} \int_0^t \frac{i(u)}{\sqrt{(t-u)}}\, du \qquad (3)$$

where I_l is convolutive current, i(u) is the current at time (u) and t is the total time of the experiment.

As indicated, I_1 convolution contains diffusional and current parts i(u) from t = 0, and reduces contributions to I_1, by scaling each current segment by a factor dependent on the time interval (t-u). It also follows that, under pure diffusion-controlled conditions [i.e., C (0, t) = 0], $I_1(t)$ exhibits its limiting value.

$$I_{lim} = nFAC\sqrt{D} \qquad (4)$$

where I_{lim} is the limiting convolution current, n is the number of electrons transferred and the remaining terms have their usual meaning.

As a result, the convolution converts CV i-E shape to an S-shaped I(t)-E curve, which has a steady-state plot and is more adjustable for data analysis, in some cases [25-28]. In addition, the sluggishness of heterogeneous kinetics or the uncompensated resistance "Ru'' does not affect I_{lim} plateau magnitude of a steady-state CV. The convolution integral $I_1(t)$ evaluation was carried out via the following algorithm [29-32]:

$$I(t) = I\,(k\Delta t) = \frac{1}{\sqrt{\pi}} \sum_{j=1}^{j=k} \frac{\Gamma\left(k-j+\frac{1}{2}\right)}{(k-j)} \Delta t 1/2 i(j\Delta t) \qquad (5)$$

where k is a variable between 0 and N, $\Delta t = t_f/N$, N representing t = 0 and t = t_f indexed by j, at Δt equally spaced time intervals, I(jΔt) is current, and Γ(x) is x Gamma function.

Fig. 4 indicates a moderate separation between forward and backward scans.

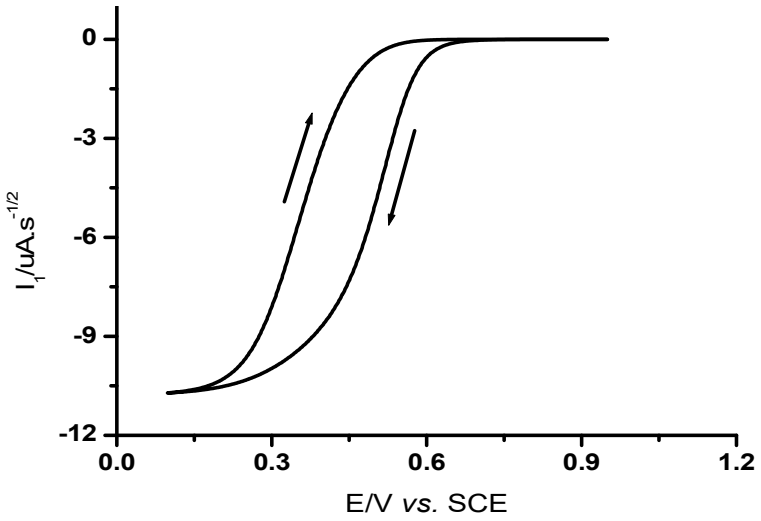

Figure 4: 0.01 M Fe (III)/Fe (II) system I_1 convolution at 0.2 V/s^{-1}.

This confirms quasi-reversibility of electrons transfer rate, and verifying the ability of CvV to determine and elucidate charge transfer rate without calculating heterogeneous rate constant.

Herein, a novel method for extracting E^o value for a quasi-reversible system from a CV and $I_l(t)$ convolution is described. As shown in Fig. 5, on the reverse sweep, current passes through zero potential ($E_{(I=0)}$). At this potential, convoluted current is given by $I_{l=0}$. Regardless of electrons transfer kinetics, the convolution relationship is reduced to its simple polarographic form at this zero current point.

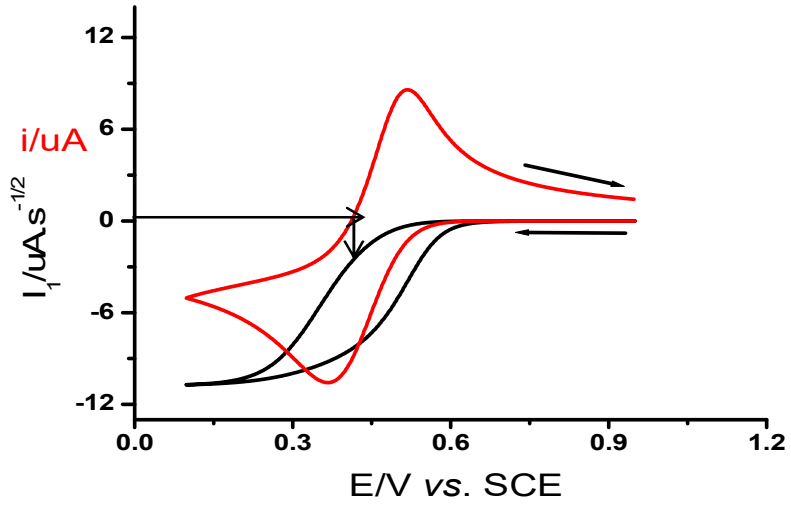

Figure 5: E^o calculation from non-Nernstian Fe (III)/Fe (II) system.

E^o value determined via this method was found to be 0.435 V. This value agrees with the one determined from CV which is mentioned in Table 2.

$$I_l - I_1 \{1 + \exp(nF/RT)[E_{i=0} - E_{1/2}]\} = 0 \quad (6)$$

on rearranging:

$$E_{1/2} = E_{i=0} + \frac{RT}{nF} \ln \frac{Il - I1}{Il} \quad (7)$$

DV

As described by [33-35], dI_1/dt was established as the E feature for a fast electron system.

$$e_p = (dI_1/dt) = nFAC\sqrt{D}\, a\zeta / (1+\zeta)^2 \quad (8)$$

where the symbol $a = n\upsilon F/RT$ and $\zeta = \exp[nF/RT (E - E^0)]$.

Fig. 6 illustrates this eq., for the way Fe (III) undergoes reduction at Au electrode.

The w_p magnitude at half height was found to be in the range from 120 to 185 mV, which demonstrates the charge transfer slow speed. Also, lack of symmetry of onward and reversed peaks indicates electrons transfer quasi-reversibility. From the

above, it is obvious that I_1 *vs.* E and dI_1/dt *vs.* E curves were easier to use, in order to offer proper information on the character of the electrode response, than i vs. E curve. D factor was further determined from eq. (6) [33, 34, 36].

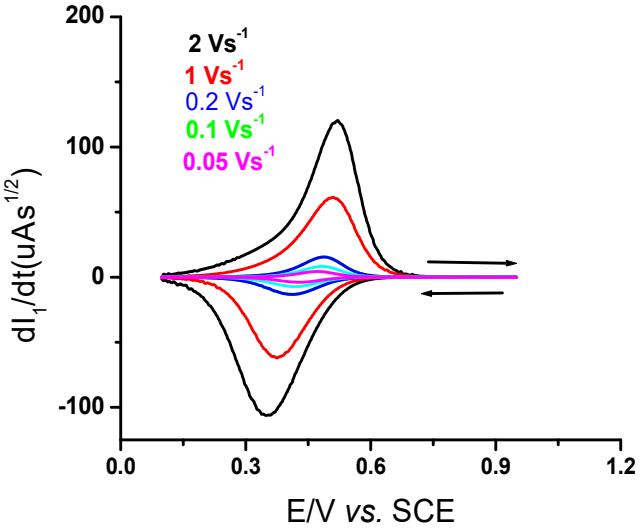

Figure 6: DV of 10^{-2} M Fe (III) ion in 1 M HCl, at Au electrode, various υ and T of 25 ºC.

D value magnitude obtained from Eq. (6) is listed in Table 2.

Table 2: Values of kinetic parameters of 0.01 M Fe (III) ions determined from different techniques at Au electrode.

Technique	D x 10^{10} (m^2/s^{-1})	E^o (V)	α	k_s x 105 m/s^{-1}
CV	4.9	0.440	0.39	2.3
CvV	5.1	0.435	---	---
DV	5.0	0.437	0.39	---
*Sim.	4.8	0.430	0.40	2.4

* Numerical simulation

Also, the arrangement between convolution and deconvolution transformations yields the following relationship:

$$n = 0.086/I_{lim}\alpha\upsilon \qquad (9)$$

where n is the number of charges consumed in the electrode pathway, with alternative parameters ordinary definitions. From eq. (7), total involved n was found to be 1.02 *ca.* 1.

Numerical simulation

A numerical simulation of simple electrons transfer was performed to determine the precise type of electrode reaction and confirm electrochemical parameters values.

Fig. 7 displays the numerical reductive CV of simple electrons transfer (E) via the following electrochemical parameters: $k_s = 2.40 \times 10^{-5}$ m/s^{-1}; $E_o = 0.43$ V; $\alpha = 0.40$; $D = 4.8 \times 10^{-10}$ m^2/s^{-1}; and n = 1.

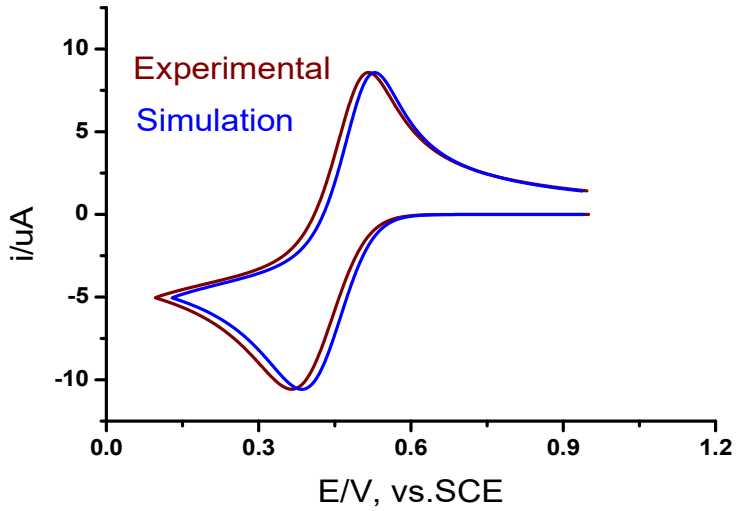

Figure 7: Comparison of numerical and experimental CV of 0.01 M *Fe* (III) ions at a SR of 0.2 V/s^{-1} and T of 25 ºC.

As shown in Fig. 7, good agreement between simulated and experimental CV confirmed the accuracy of the determined electrochemical parameters for *Fe* (III) ion.

Conclusion

In this report, the chemistry of *Fe* (III) /*Fe* (II) systems was explained at a working Au electrode in a 1 M HCl aqueous solution using CV, CvV and DV experiments. The proper parameters of the investigated system were experientially computed and theoretically validated via the numerical simulation method.

Authors' contributions

I. S. El-Hallag: suggested the idea of the present article; illustrated obtained results; wrote the manuscript. **A. A. Al-Owais**: performed experimental work and numerical simulation.

Abbreviations

A: surface electrode area (cm^2)
Ag/AgCl: silver/silver chloride
Au: gold
C: bulk concentration of electroactive species (mol/L)
CV: cyclic voltammetry
CvV : convolution voltammetry

D: diffusion coefficient (cm^2)
$dI1/dt = d^{1/2}i/dt^{1/2}$: semi-differentiation of current
DNA: deoxyribonucleic acid
DV: deconvolution voltammetry
E^o: standard redox potential (V)
$E_{1/2}$: half-wave potential (V)
e_p: (dI_1/dt): height of deconvoluted peak current
E_{pa}: anodic peak potential (V)
$E_{pa} - E_{pc}$: peak potential separation (V)
E_{pc}: cathodic peak potential (V)
F: Faraday's constant (96500 $C.mol^{-1}$)
Fe (II): ferrous ion
Fe (III): Ferric ion
$FeCl_3$: ferric chloride
$FeSO_4$: ferrous sulfate
FRAP: Fe (III) reducing antioxidant power
HCl: hydrochloric acid
I_{conv}: convolution current
i_{deconv}: deconvolution current
i**-E curve**: current-potential curve
I_{lim}: limiting convoluted current ($\mu A/s^{-1/2}$)
i_p: peak current
i_{pa}: height of anodic peak current (μA)
i_{pc}: height of cathodic peak current (μA)
$K_3[Fe(CN)_6]$: potassium ferricyanide
KNO_3: potassium nitrate
k_s: heterogeneous rate constant (cm/s^{-1})
n: number of electrons involved in the electrode reaction
NHFe: non-heme Fe
R: universal gas constant, (8.314 $J/mol^{-1}/K^{-1}$)
Redox: reduction-oxidation reaction
Sim: digital simulation
SR: scan rate
T: absolute temperature (K)
w_p: peak width of the deconvolution peak height (V)

Symbols definition

α: transfer coefficient
υ: scan rate (V/s)

References

1. Abbaspour N, Hurrell R, Kelishadi R. Review on iron and its importance for human health. J Res Med Sci. 2014;(19):164-174.

2. Koskenkorva-Frank TS, Weiss G, Koppenol WH et al. The complex interplay of iron metabolism, reactive oxygen species, and reactive nitrogen species: insights into the potential of various iron therapies to induce oxidative and nitrosative stress. Free Radic Biol Med. 2013;(65):1174-1194. https://doi.org/10.1016/j.freeradbiomed.2013.09.001
3. Liu H, Yu Q, Ma Y et al. Cyclic voltammetry: A simple method for determining contents of total and free iron ions in sodium ferric gluconate complex. J Electrochem Sci Engi. 2020;(10)3:281-291. https://dx.doi.org/10.5599/jese.749
4. Geisser P, Burckhardt S. The Pharmacokinetics and Pharmacodynamics of Iron Preparations. Pharmaceutics. 2011;(3):12. https://doi.org/10.3390/pharmaceutics3010012
5. Waldvogel-Abramowski S, Waeber G, Gassner C et al. Physiology of iron metabolism. Transfus Med Hemotherap. 2014;41:213-221. https://doi.org/10.1159/000362888
6. Chen CY, Berish SA, Morse SA et al. The ferric iron-binding protein of pathogenic *Neisseria* spp. functions as a periplasmic transport protein in iron acquisition from human transferrin. Mol Microbiol. 1993;10:311-318. https://doi.org/10.1111/j.1365-2958.1993.tb01957.x
7. Hemadi M, Ha-Duong NT, El Hage-Chahine JM. The mechanism of iron release from the transferrin-receptor 1 adduct. J Mol Biol. 2006;358:1125-1136. https://doi.org/10.1016/j.jmb.2006.02.055
8. Geisser P, Burckhardt S. The pharmacokinetics and pharmacodynamics of iron preparations. Pharmaceutics. 2011;3:12-33. https://doi.org/10.3390/pharmaceutics3010012
9. Waldvogel-Abramowsk S, Waeber G, Gassner C et al. Physiology of iron metabolism. Transfus Med Hemotherap. 2014;41:213-221. https://doi.org/10.1159/000362888
10. Conrad ME, Umbreit JN, Moore EG et al. Separate pathways for cellular uptake of ferric and ferrous iron. Amer J Physiol Gastrointest Liver Physiol. 2000;279:767-774. https://doi.org/10.1152/ ajpgi.2000. 279.4.G767
11. Ouameur AA, Arakawa H, Ahmad R et al. Comparative Study of Fe(II) and Fe(III) Interactions with DNA Duplex: Major and Minor Grooves Bindings. DNA Cell Biol. 2005;24:94-401. https://doi.org/10.1089/dna.2005.24.394
12. Babu KF, Kumar RS, Kulandainathan MA et al. Ferric-oxalate-gluconate based redox mediated electrochemical system for vat dyeing. J Appl Electrochem. 2009;39:1025-1031. https://doi.org/10.1007/ s10800-008-9750-9
13. Bechtold T, Turcanu A. Fe^{3+}--gluconate and Ca^{2+}-Fe^{3+}-gluconate complexes as mediators for indirect cathodic reduction of vat dyes – Cyclic voltammetry and batch electrolysis experiments. J Appl Electrochem. 2004;34:1221-1227. https://doi.org/10.1007/s10800-004-1707-z
14. Wong CSM, Kwok JC, Richardson DR. PCTH: a novel orally active chelator of the aroylhydrazone class that induces iron excretion from mice. Biochimic Biophys Acta Mol Basis Disea. 2004;1793;70-80. https://doi.org/10.1016/j.bbadis.2004.09.001

15. Bridgea MH, Williams E, Michael EG et al. Electrochemical investigation into the redox activity of Fe(II)/Fe(III) in the presence of nicotine and possible relations to neurodegenerative diseases. Biochim Biophysic Acta Mol Basis Disea. 2004;1690:77-84. https://doi.org/10.1016/j.bbadis.2004.05.007
16. Mohr S, Bechtold T. Electrochemical behaviour of iron-complexes in presence of competitive ligands: A strategy for optimization of current density. J Appl Electrochem. 2001;31:363-368. https://doi.org/10.1023/A:1017536204530
17. Rudnik E. Effect of gluconate ions on electroreduction phenomena during manganese deposition on glassy carbon in acidic chloride and sulfate solutions. J Electroanalyt Chem Interfac Electrochem. 2015;741:20-31. https://doi.org/10.1016/j.jelechem.2015.01.019
18. Rudnik E, Wojnicki M, Włoch G. Effect of gluconate addition on the electrodeposition of nickel from acidic baths. Surf Coat Technol. 2012;207:375-388. https://doi.org/10.1016/j.surfcoat.2012.07.027
19. Moharram YI. Extraction of electrode kinetics and transport parameters of ferrocene at a platinum electrode from semi integral electroanalysis. J Electroanalyt Chem Interfac Electrochem. 2006;(1)587:115-126. https://doi.org/10.1016/j.jelechem. 2005.10.024
20. Moharram YI, Ghoneim MM. Determination of the kinetic parameters of ferrocene-N-phenylaza-15-crown-5 by methods of convolution electrochemistry. J Electroanalyt Chem Interfac Electrochem. 2004;(1)570:135-143. https://doi.org/10.1016/j.jelechem.2004.03.025
21. Moharram YI. Determination of the chemical and electrochemical parameters for a CE system by methods of convolution electrochemistry. J Electroanalyt Chem Interfac Electrochem. 2004;563:283-290. https://doi.org/10.1016/j.jelechem.2003.07.044
22. Bolinger RW. The Deployment of Digital Simulation Tools to Verify Cyclic Voltammetry Experiments. PhD Thesis, ETH Zürich (2000).
23. Demortier A, Jehoulet C. Digital simulation of cyclic voltammetric curves when the oxidized and the reduced forms of a redox couple are present in solution. J Electroanalytic Chem. 1990;283:15-33. https://doi.org/10.1016/0022-0728(90)87376-U
24. Plambeck JA. Electroanalytical chemistry: Basic Principles and Applications, John Wiley & Sons, New York, Chichester, Brisbane, Toronto, Singapore, 1982:404.
25. Banks CE, Davies TJ, Wildgoose GG et al. Electrocatalysis at graphite and carbon nanotube modified electrodes: edge-plane sites and tube ends are the reactive sites. Chem Commun. 2005;7:829-841. https://doi.org/10.1039/B501179P
26. Watkins JD, Lawrence K, Taylor JE et al. Carbon Nanoparticle Surface Electrochemistry: High-Density Covalent Immobilisation and Pore-Reactivity of 9,10-Anthraquinone. Electroanalysis. 2011;23:1320-1324. https://doi.org/10.1002/elan.201100051

27. Sadowska K, Roberts KP, Wiser R et al. Synthesis, characterization, and electrochemical testing of carbon nanotubes derivatized with azobenzene and anthraquinone. Carbon. 2009;47:1501. https://doi.org/10.1016/j.carbon.2009.01.044
28. Laviron E. General expression of the linear potential sweep voltammogram in the case of diffusionless electrochemical systems. J Electroanalyt Chem Interfac Electrochem. 1979;101:19-28. https://doi.org/10.1016/S0022-0728(79)80075-3
29. Al-Owais AA, El-Hallag IS, El-Mossalamy EH. Electrochemical investigation of anthracen-9-ylmethylene-(3,4- dimethyl-isoxazol-5-yl)-amine compound at gold electrode. Int J Electrochem Sci. 2022;17:220917. https://doi.org/10.20964/2022.09.19
30. Wong EH, Kabbani RM. Boron halide clusters and radicals: synthesis and interconversions of the three oxidation states of a nine-boron polyhedron. Inorg Chem. 1980;19:451-455. https://doi.org/10.1021/ic50204a033
31. Galvez J, Su J, Park M. Pulse polarography: theory for the current-potential curves of an EE mechanism. J Electroanalyt Chem Interfac Electrochem. 1987;235:71-85. https://doi.org/10.1016 /0022-0728(87)85198-7
32. Saveant JM, Tessier D. Convolution potential sweep voltammetry V. Determination of charge transfer kinetics deviating from the Butler-Volmer behaviour. J Electroanalyt Chem Interfac Electrochem. 1975;65:57-66. https://doi.org/10.1016/0368-1874(75)85105-7
33. Ghoneim MM, El-Hallag IS. Electrochemical Investigation of Some Ruthenium-Carborane Complexes at a Glassy Carbon Electrode. Monatsh Chem. 1999;130:525-535. https://doi.org/10.1007/PL00010231
34. Al Owais AA, El-Hallag IS, El-Mossalamy E. Voltammetric investigation of electrooxidation of Methyl(E)-2- cyno(N-ethyl carbazol-2-yl) acrylate at a gold electrode. Int J Electrochem Sci. 2022;17:220821. https://doi.org/ 10.20964/2022.08.08
35. AL-Owais AA, El-Hallag IS. Voltammetric Studies of Catechol Behavior in Presence of 4,4'- bipyridine via Convolutive Voltammetry, Chronoamperometry and Digital Simulation. Int J Electrochem Sci. 2021;(16):210637. https://doi.org/10.20964/2021.06.58
36. Ghanem MA, El-Hallag IS, Amer MS et al. Characteristics of the voltammetric behavior of the hydroxide ion oxidation at disordered mesoporous titanium dioxide electrocatalyst. J Saudi Chem Soc. 2021;25:101274. https://doi.org/ 10.1016/j.jscs.2021.101274